Two-Dimensional Power Allocation for Optical MIMO-OFDM Systems Over Low-Pass Channels

Xiong Deng, *Member, IEEE*, Wenxiang Fan, Thiago E. Bitencourt Cunha, *Member, IEEE*, Shuai Ma, *Member, IEEE*, Chen Chen, *Member, IEEE*, Yixian Dong, Xihua Zou, *Senior Member, IEEE*, Lianshan Yan, *Senior Member, IEEE*, and Jean-Paul M. G. Linnartz, *Fellow, IEEE*

***Abstract*—Multiple-input multiple-output (MIMO) combined with orthogonal frequency-division multiplexing (OFDM) technique can dramatically increase the achievable rate of visible light communication (VLC) systems. The channel in a VLC system with light-emitting diode (LED) luminaires is generally low-pass, which highly limits the achievable rate of practical VLC systems. This aspect has largely been ignored in the analysis for MIMO-OFDM VLC systems. As wide parts of the bandwidth at higher frequencies are severely attenuated, the choice of the power loading on every frequency bin has a large impact on the achieved bit rate. Thus, in this paper, we propose a two-dimensional water-filling (2D-WF) power allocation algorithm that operates both in frequency and space domains to efficiently improve the rate achieved by MIMO-OFDM VLC systems over low-pass VLC channels. The achievable rates and optimal bandwidths of a MIMO-OFDM VLC system are derived analytically using the proposed 2D-WF power allocation algorithm and five conventional power allocation strategies, including uniform (UF) power allocation, pre-emphasis (PE) power allocation, beamforming (BF) power allocation, and two kinds of one-dimensional water-filling (1D-WF) power allocation. Our simulation results show that the achievable rate of a MIMO-OFDM VLC system in a typical indoor environment can be significantly degraded by the low-pass effect. The proposed 2D-WF power allocation outperforms all other schemes in terms of achievable bit rate.**

***Index Terms*—MIMO, OFDM, VLC, water-filling power allocation, low-pass channel, achievable rate.**

Manuscript received November 6, 2021; revised February 19, 2022; accepted March 20, 2022. Date of publication March 31, 2022; date of current version July 18, 2022. This work was supported in part by the China National Key R&D Programmes under Grants 2021YFB2800801 and 2021YFB2800305, in part by the National Natural Science Foundation of China under Grants 62001174, 61901065, and 62101465, in part by the Sichuan Outstanding Youth Science and Technology Talents Project under Grant 2022JDJQ0047, in part by Sichuan Science and Technology Program under Grant 2022JDTD0013, and in part by the European H2020 Project Enhance Lighting for the Internet of Things (ELIoT), under Grant 825651. The review of this article was coordinated by Dr. Sudhan Majhi. *(Corresponding author: Wenxiang Fan)*

Xiong Deng is with the Center for Information Photonics and Communications, Southwest Jiaotong University, Chengdu 610031, China, and also with the Department of Electrical Engineering, Eindhoven University of Technology, 5600 MB Eindhoven, The Netherlands (e-mail: xiongdeng@swjtu.edu.cn).

Wenxiang Fan is with the Center for Information Photonics and Communications, Southwest Jiaotong University, Chengdu 610031, China, and also with the Institute of Electronic Paper Displays, South China Academy of Advanced Optoelectronics, South China Normal University, Guangzhou 510006, China (e-mail: wxfan@m.scnu.edu.cn).

Thiago E. Bitencourt Cunha is with the Department of Electrical Engineering, Eindhoven University of Technology, 5600 MB Eindhoven, The Netherlands (e-mail: t.e.bitencourt.cunha@tue.nl).

Yixian Dong, Xihua Zou, and Lianshan Yan are with the Center for Information Photonics and Communications, Southwest Jiaotong University, Chengdu 610031, China (e-mail: ydong@swjtu.edu.cn; zouxihua@swjtu.edu.cn; lsyan@home.swjtu.edu.cn).

Jean-Paul M. G. Linnartz is with the Department of Electrical Engineering, Eindhoven University of Technology, 5600 MB Eindhoven, The Netherlands, and also with the Signify (Philips Lighting) Research, 5656 AE Eindhoven, Netherlands (e-mail: Linnartz,j.p.linnartz@signify.com).

Shuai Ma is with the School of Information and Control Engineering, China University of Mining and Technology, Xuzhou 221116, China (e-mail: mashuai001@cumt.edu.cn).

Chen Chen is with the School of Microelectronics and Communication Engineering, Chongqing University, Chongqing 400044, China (e-mail: c.chen@cqu.edu.cn).

Digital Object Identifier 10.1109/TVT.2022.3162621

I. Introduction

VISIBLE light communication (VLC) utilizes light-emitting diode (LED) luminaires lighting and has drawn significant interest due to the dual-function of illumination and data transmission [1]. An LED-based VLC system has many other advantages such as low cost, high security, license free and silence to electromagnetic interference, which is well positioned as the potential key technology for the new 6G communication [2]. The momentum of next generation 6G and Internet of things (IoT) devices such as autonomous vehicles and robots, industry 4.0, virtual or augmented reality, drives the demand for high wireless capacity. However, there is a severe challenge for LED-based VLC systems as the bandwidth of white LEDs is only several MHz due to the LED junction capacitance [3] and color-converting phosphors [4]. These limit the throughput of LED-based VLC systems. However, orthogonal frequency division multiplexing (OFDM) allows efficient use of modulation frequencies that go far beyond the 3 dB bandwidth of the LED and the phosphor, by optimally allocating power and bits at each frequency bin.

Multiple-input multiple-output (MIMO) is an other technique to boost spectrum efficiency. It has become a vital solution to achieve high data rates. MIMO techniques are widely applied in radio frequency (RF) communication systems. In indoor environments, lighting is usually implemented via multiple LEDs located at different locations to obtain uniform illumination [5]. Hence, distributed-MIMO becomes a natural technique in VLC systems [6], [7], which is able to retain communication even if one light of sight (LoS) path is blocked. Compared to single-input single-output (SISO) VLC systems, MIMO-VLC systems over space channels have been proven to be able to dramatically increase the achievable rate [8]. Thus, MIMO combined with OFDM technique promises to be a natural combination and key

0018-9545 © 2022 IEEE. Personal use is permitted, but republication/redistribution requires IEEE permission.
See https://www.ieee.org/publications/rights/index.html for more information.

Authorized licensed use limited to: CHONGQING UNIVERSITY. Downloaded on July 16,2022 at 07:24:30 UTC from IEEE Xplore. Restrictions apply.

technique to effectively enhance the rate and communication reliability of VLC systems, particularly in an indoor environment. In LED-based MIMO-OFDM VLC systems, there are two dimensions over which to allocate power, namely among the OFDM sub-carriers in frequency domain and across the multiple spatial streams. A hybrid space-frequency domain pre-equalization has shown better performance than the system using only frequency domain pre-equalization [9]. LED-based MIMO-OFDM VLC systems have already been experimentally demonstrated to achieve high data rate in [10], [11], but they did not consider allocating the optimal power and bits at each sub-channel or sub-carrier.

The channel in VLC system is generally low-pass [12], [13], which has been largely ignored in the analysis for VLC systems. The low-pass nature nonetheless appears to have a significant impact [14]–[16]. In literature, we see three models for the low-pass frequency channel response: Gaussian, exponential and first-order low-pass models. The Gaussian low-pass model has been experimentally demonstrated to closely match with a step-index plastic optical fiber over intensity-modulation/direct-detection (IM/DD) optical channel, where the noise is additive white Gaussian noise (AWGN) [17]. The exponential model is an empirical expression that has been experimentally demonstrated to closely match with the measured LED communication low-pass channel response [18], [19]. The first-order model has a physical foundation for phosphor–coated blue LEDs in [20] and also for LEDs which have a quantum-well with a fairly constant concentration of holes and electrons [12]. For LEDs in which the distribution of charge carriers is less uniform, the 3 dB point is smeared across a wider range of frequencies, and apparently [19] the exponential model described this reasonably well in practice. Thus, we adopt the exponential low-pass channel model in the analysis on the MIMO-OFDM VLC system.

MIMO-VLC systems can be generally divided into two categories based on whether imaging lens is used: imaging MIMO and non-imaging MIMO [8]. There are generally three transmission modes of MIMO, i.e., spatial diversity (SD) [21], spatial multiplexing (SMP) [22], and spatial modulation (SM) [11]. Under SD and SMP modes, a diversity gain and multiplexing gain can be obtained for MIMO-VLC systems respectively [23], while under SM mode, extra bits by spacial index-modulation can be transmitted along with a traditional constellation diagram for throughput increment [24]. In this work, we consider non-imaging MIMO with the stream scheme of SMP. Besides, a general indoor VLC system has two types of propagation modes between transmitters and receivers, including LoS propagation and diffuse propagation. The literature suggests that the power received over the diffuse propagation is much lower than that of LOS propagation [8], [25]. Hence, only LoS propagation is considered in this work. To guarantee the transmitted signals to be positive, direct current biased optical OFDM (DCO-OFDM) adds a DC-offset in the signals and clips the remaining negative signals to zero [26]. Other OFDM variants such as Asymmetric Clipped Optical OFDM (ACO-OFDM), Pulse Amplitude Modulated OFDM (PAM-OFDM) or Flip OFDM avoid the inefficient DC bias power so as to improve the energy efficiency, but at a price in bandwidth utilization. In this work, we mainly consider DCO-OFDM and the power allocation strategy can be also applied to other OFDM forms.

It is vital to assign the most appropriate power to each LED, which not only saves energy but also increases the throughput. To this end, we adopt the singular value decomposition (SVD)-based technique to decompose the MIMO-OFDM VLC channel into independent parallel sub-channels as reported in [29]. Although in [31] the performance of a MIMO-OFDM VLC system was investigated with adaptive bit and power allocation, the low-pass effect was not taken into account. Recently, we investigated the low-pass effect in the MIMO-VLC system using numerical CVX optimization [15], but we continued to search for insightful expressions. In this work, we further propose an efficient two-dimensional water-filling (2D-WF) power allocation algorithm to improve the achievable rate of MIMO-OFDM VLC systems over low-pass channels. The preliminary results were presented in [32]. For a comparison, the achievable rate and optimal normalized bandwidths calculations with five conventional power allocation strategies, including uniform (UF) power allocation, two kinds of one-dimension water-filling (1D-WF) power allocation, pre-emphasis (PE) power allocation and beamforming (BF) power allocation [30], are also analyzed over the low-pass channels.

For clarity, we have provided a detailed comparison between existing related works and our work in Table I. The main contributions of this paper can further be summarized as follows:

- With an SVD-based technique, we analyze the signal processing process of a typical MIMO-OFDM VLC system over low-pass channels, and derive the overall achievable rate of the proposed system.
- Based on our derived expression for achievable rate, we propose a 2D-WF power allocation strategy over both the spatial and the frequency domains to maximize the rate of the MIMO-OFDM VLC system over low-pass channels. A closed-form expression is obtained for the performance by our proposed 2D-WF power allocation strategy. Then, we propose an algorithm to achieve the optimal results.
- Under the total transmit power constraint, the achievable rates and optimal bandwidths of a MIMO-OFDM VLC system over low-pass channels are derived analytically with five conventional power allocation strategies.
- Extensive analytical and simulation results are presented to evaluate and compare the performance of a MIMO-OFDM VLC system over low-pass channels with different power allocation strategies in two cases of typical indoor environment. The obtained results demonstrate the good performance of the proposed 2D-WF power allocation strategy.

The remainder of this paper is organized as follows. In Section II, we describe the model of a general MIMO-OFDM VLC system over the low-pass channels. In Sections III, the achievable rates and optimal normalized bandwidths of the MIMO-OFDM VLC system with the proposed 2D-WF power allocation strategy and other five conventional power allocation strategies are derived, respectively. In Section IV, simulations are performed and the results are discussed. Section V draws conclusions from this paper.

Authorized licensed use limited to: CHONGQING UNIVERSITY. Downloaded on July 16,2022 at 07:24:30 UTC from IEEE Xplore. Restrictions apply.

TABLE I
THIS WORK IN COMPARISON WITH THE RELATED WORKS

Ref.	MIMO/SISO	Low-pass model	Space domain WF[1]	Frequency domain WF	Space-frequency domain WF	UF[2]	PE[3]	BF[4]
[18]	SISO	Exponential	No[5]	Yes[6]	No	Yes	No	No
[19]	SISO	Exponential	No	Yes	No	Yes	Yes	No
[20]	SISO	First-order	No	Yes	No	Yes	No	No
[27]	SISO	Gaussian	No	Yes	No	Yes	No	No
[28]	SISO	First-order & Gaussian	No	Yes	No	No	No	No
[7]	MIMO	N.A.[7]	No	No	No	Yes	No	No
[9]	MIMO	N.A.	No	No	No	No	Yes	No
[10]	MIMO	N.A.	No	No	No	Yes	No	No
[23]	MIMO	N.A.	No	No	No	Yes	No	No
[25]	MIMO	N.A.	No	Yes	No	No	No	No
[29]	MIMO	N.A.	Yes	No	No	No	No	No
[30]	MIMO	N.A.	Yes	No	No	No	No	Yes
This work	MIMO	Exponential	Yes	Yes	Yes	Yes	Yes	Yes

[01] Water-filling. [2] Uniform. [3] Pre-emphasis. [4] Beam-forming. [5] Not consider. [6] Consider. [7] Not Applicable.

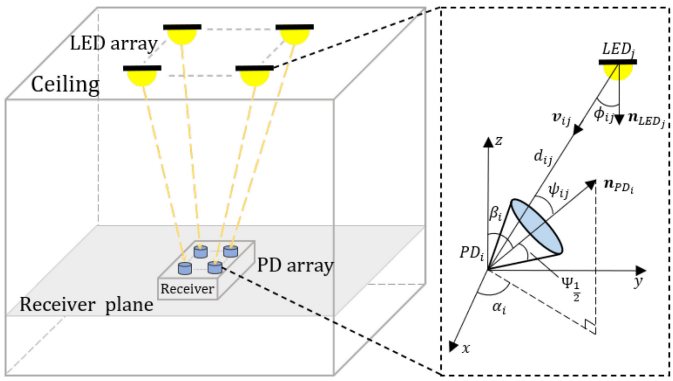

Fig. 1. Geometric representation of the $N_R \times N_T$ MIMO VLC system.

Notation: Scalars, vectors, and matrices are respectively denoted by non-boldface italic letters, lowercase boldface letters, and capital boldface letters. The operators $(\cdot)^T$ and $(\cdot)^H$ represent the transpose and the conjugated transpose of a vector or matrix, respectively. $||\cdot||$ denotes the norm of a vector.

II. SYSTEM MODEL

In this section, we describe a MIMO-OFDM VLC system with N_T LEDs and N_R photodiodes (PDs), where IM/DD with DCO-OFDM is considered. The described system is illustrated in Fig. 1.

After the LoS propagation, the received electrical signal by the user can be written as

$$\mathbf{y}(f) = \mathbf{H}(f)\mathbf{x}(f) + \mathbf{n}(f), \tag{1}$$

where $\mathbf{y}(f) = [y_1(f), y_2(f), \ldots, y_{N_R}(f)]^T$, for $f \in [0, f_{\max}]$, where $f_{\max}$ is the maximal used bandwidth, denotes the $N_R \times 1$ received signal vector at the f-th sub-carrier. $\mathbf{x}(f) = [x_1(f), x_2(f), \ldots, x_{N_T}(f)]^T$ is the transmitted signal vector, and $\mathbf{n}(f) = [n_1(f), n_2(f), \ldots, n_{N_R}(f)]^T$ is the $N_R \times 1$ AWGN vector whose entries are zero-mean independent and identically distributed (i.i.d) Gaussian random variables with variance $\sigma_n^2 = N_0 B$, where N_0 is the power spectral density (PSD) of the noise and B is the noise bandwidth [33].

$\mathbf{H}(f)$ represents the channel frequency response matrix. As discussed previously, in this work, only LoS propagation is considered. In this case, we can model each MIMO channel with a constant channel DC gain over all frequency range and the frequency-selectivity which is related to the low-pass nature of LEDs [34]. Thus, the channel frequency response matrix $\mathbf{H}(f)$ can be expressed by

$$\mathbf{H}(f) = \begin{bmatrix} h_{11}(0)h_{11}(f) & \cdots & h_{1N_T}(0)h_{1N_T}(f) \\ \vdots & \ddots & \vdots \\ h_{N_R1}(0)h_{N_R1}(f) & \cdots & h_{N_RN_T}(0)h_{N_RN_T}(f) \end{bmatrix}, \tag{2}$$

where $h_{ij}(0)$, for $i = 1, 2, \ldots, N_R$ and $j = 1, 2, \ldots, N_T$, represents the DC channel gain between the j-th LED and the i-th PD, and $h_{ij}(f)$ corresponds to the low-pass frequency channel response between the j-th LED and the i-th PD. In this work, we consider that the used LEDs and PDs are identical, i.e., we adopt the same exponential low-pass channel model, thus, $h_{ij}(f) = h(f), \forall i \in [1, N_T]$ and $\forall j \in [1, N_R]$, and can be expressed as [18], [19]

$$|h(f)|^2 = 2^{-\frac{f}{f_c}}, \tag{3}$$

where f_c is the 3 dB cut-off frequency of the channel. The value of f_c varies for the different off-the-shelf LEDs, but it will not affect the power allocation strategies discussed in Section III.

So, following [16], (2) can be rewritten as $\mathbf{H}(f) = \mathbf{H}(0)h(f)$, in which $\mathbf{H}(0)$ is the $N_R \times N_T$ DC channel gain matrix. Without consideration of the effect of optics, such as a lens, the emission from an LED can be modeled by a Lambertian radiation pattern. The DC channel gain $h_{ij}(0)$ is calculated by [35]

$$h_{ij}(0) = \begin{cases} \frac{(m+1)\rho A}{2\pi d_{ij}^2} \cos^m(\phi_{ij}) \cos(\psi_{ij}), & 0 \le \psi_{ij} \le \Psi_{\frac{1}{2}}, \\ 0, & \psi_{ij} > \Psi_{\frac{1}{2}}, \end{cases} \tag{4}$$

where the coefficient $m = -\ln(2)/\ln(\cos(\Phi_{\frac{1}{2}}))$ corresponds to the order of lambertian emission, where $\Phi_{\frac{1}{2}}$ is semiangle at half power of the LED. ρ and A denote, respectively, the responsivity and the active area of the PD. d_{ij} depicts the distance between the i-th PD and the j-th LED. Furthermore, ϕ_{ij} is the angle of

Authorized licensed use limited to: CHONGQING UNIVERSITY. Downloaded on July 16,2022 at 07:24:30 UTC from IEEE Xplore. Restrictions apply.

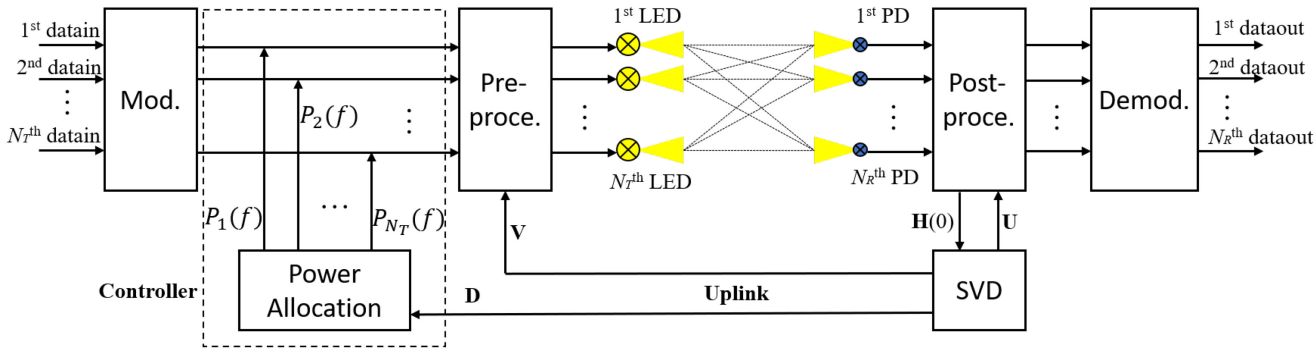

Fig. 2. Block diagram of SVD and power allocation.

emergence to the emitter axis, and ψ_{ij} is the angle of incident to the incident axis. The coefficient $\Psi_{\frac{1}{2}}$ represents the field-of-view (FOV) semiangle of the receiver. It can be observed in (4) that, due to the geometric dependence, if the emitter or detector is not in each other's FOV, the DC channel gain is negligible. These parameters are depicted in Fig. 1.

To reduce the channel correlation, i.e., enhance the quality of sub-channels, in this work, we consider that the MIMO-OFDM VLC systems adopt angle diversity receivers (ADR) [36]. Subsequently, we illustrate the ADR coordinate system in Fig. 1. As we can see, $\mathbf{l}_{LED_j}$ denotes the normal vector of the j-th LED in the direction of emission light, $\mathbf{l}_{PD_i}$ denotes the normal vector of the i-th PD in the direction of incident light, $\mathbf{v}_{ij}$ denotes the vector from the j-th LED to the i-th PD, α_i denotes the azimuth angle of the i-th PD, i.e., the angle of $\mathbf{l}_{PD_i}$ from the positive $\boldsymbol{x}$-axis, β_i denotes the elevation angle of the i-th PD, i.e., the angle of $\mathbf{l}_{PD_i}$ from the positive $\boldsymbol{z}$-axis.

Without loss of generality, the Cartesian coordinates of the j-th LED and the i-th PD can be denoted as $[x_j, y_j, z_j]$ and $[x_i, y_i, z_i]$, respectively. Consequently, $\mathbf{l}_{LED_j}$, $\mathbf{l}_{PD_i}$ and $\mathbf{v}_{ij}$ can be respectively expressed as $\mathbf{l}_{LED_j} = [0, 0, -1], \mathbf{l}_{PD_i} = [\sin\beta_i \cos\alpha_i, \sin\beta_i \sin\alpha_i, \cos\beta_i], \mathbf{v}_{ij} = [x_i - x_j, y_i - y_j, z_i - z_j]$.

Following above discussion, the cosine of the emission angle and the incident angle can be respectively calculated by

$$\cos(\phi_{ij}) = \frac{\mathbf{l}_{LED_j} \cdot \mathbf{v}_{ij}^T}{||\mathbf{l}_{LED_j}|| \cdot ||\mathbf{v}_{ij}||} = \frac{z_j - z_i}{[(x_i - x_j)^2 + (y_i - y_j)^2 + (z_i - z_j)^2]^{1/2}},$$

$$\cos(\psi_{ij}) = \frac{\mathbf{l}_{PD_i} \cdot -\mathbf{v}_{ij}^T}{||\mathbf{l}_{PD_i}|| \cdot || - \mathbf{v}_{ij}||} \tag{5}$$

$$= \frac{[(x_j - x_i)\cos\alpha_i + (y_j - y_i)\sin\alpha_i]\sin\beta_i + (z_j - z_i)\cos\beta_i}{[(x_i - x_j)^2 + (y_i - y_j)^2 + (z_i - z_j)^2]^{1/2}}. \tag{6}$$

Next, the achievable rate expression of the proposed system is derived.

The block diagram of the operation of SVD is illustrated in Fig. 2. Channel state information (CSI) is generally utilized for MIMO demultiplexing as mentioned in [23]. For instance, a time-multiplexed training approach can be employed in MIMO-VLC systems for efficient CSI estimation [37]. It has been shown [16] that in LED based MIMO scenarios the channel matrix can described well by the concatenation of a frequency-independent crosstalk matrix (originating from overlapping radiation patterns) and a frequency response that is identical for all streams and all channels (mainly caused by the low-pass nature of LED, photodiodes possibly partially compensated by pre-emphasizing electronics). These insights reveal that the number of parameter that dynamically vary are very small, and are in practice mainly the frequency-independent change in overlap. These can easily be tracked with little signalling overhead and only limited number of pilot tones. This, in contrast to the case for RF, allows accurate tracking of the channel variations. The multipath reception that characterizes RF communication would require the estimation of many parameters in frequency domain (particularly with longer delay spreads) and in time domain (typically every time the antenna moves over 1/6 of a wavelength). Since CSI estimation is not the focus of this manuscript and imperfect CSI will not affect our analysis in VLC, we assume that the transmitter and receiver both perfectly know the CSI $\mathbf{H}(0)$.

To obtain the independent parallel sub-channels, we assume that $N_T \leq N_R$, and follow the SVD of the channel matrix $\mathbf{H}(0)$, $\mathbf{H}(0) = \mathbf{U}\mathbf{D}\mathbf{V}^H$, where $\mathbf{U}$ and $\mathbf{V}$ are $N_R \times N_T$ and $N_T \times N_T$ unitary matrices, respectively. $\mathbf{D} = diag\{\sqrt{\lambda_1}, \sqrt{\lambda_2}, \ldots, \sqrt{\lambda_k}\}$, for $k = 1, 2, \ldots, K$, is a $N_T \times N_T$ diagonal matrix, where $\sqrt{\lambda_k}$ corresponds to the singular values of $\mathbf{H}(0)$, and K is the rank of $\mathbf{H}(0)$, hence, $K = N_T$.

Following the above discussion, (1) can be rewritten as

$$\mathbf{y}'(f) = \mathbf{D}h(f)\mathbf{x}'(f) + \mathbf{n}'(f), \tag{7}$$

where $\mathbf{y}'(f) = \mathbf{U}^H\mathbf{y}(f)$, $\mathbf{x}'(f) = \mathbf{V}^H\mathbf{x}(f)$ and $\mathbf{n}'(f) = \mathbf{U}^H\mathbf{n}(f)$, i.e., the transformation $\mathbf{V}^H$ multiplexes the transmit signals, and the transformation $\mathbf{U}^H$ demultiplexes the receive signals. Then, the MIMO channel can be decomposed into independent equivalent sub-channels. Therefore, the matrices, $\mathbf{V}$ and $\mathbf{U}$, can also represent the pre-processing matrix at the transmitter and the post-processing matrix at the receiver, respectively [29], as shown in Fig. 2. It should be noted that, despite the decomposition, the statistical properties of both $\mathbf{x}'(f)$ and $\mathbf{n}'(f)$ remain the same.

Authorized licensed use limited to: CHONGQING UNIVERSITY. Downloaded on July 16,2022 at 07:24:30 UTC from IEEE Xplore. Restrictions apply.

Thus, the MIMO channel can be decomposed into independent parallel sub-channels and expressed as

$$y'_k(f) = \sqrt{\lambda_k} h(f) x'_k(f) + n'_k(f). \tag{8}$$

Following (8), for a given BER, the achievable rate, i.e., spectrum efficiency in bits/s/Hz of the k-th equivalent sub-channel of LED-based MIMO-OFDM VLC system over low-pass channels can be represented by [19]

$$R_k = \int_0^{f_{\max}} \alpha \log_2 \left(1 + \frac{\lambda_k P_k(f)}{a\Gamma N_0} 2^{-\frac{f}{f_c}}\right) df, \tag{9}$$

where the parameter α is a spectral efficiency scaling factor, and for DCO-OFDM based MIMO-VLC systems $\alpha = 1$ [38]. $f_{\max}$ is the maximal used bandwidth of each sub-channel, which may be different for different sub-channels. $a = 2\pi/e$ is a correction factor for VLC model in which input signals are real and nonnegative [39]. The rate in (9) resembles the Shannon capacity expression for real–valued power–limited linear and time Invariant (LTI) additive white Gaussian noise (AWGN) channels, which the LED channel may not be. The modulation gap Γ can be interpreted as the distance that a practical modulation scheme has from the capacity expression of such an ideal channel ($\Gamma \geq 1$) [19]. Its use can be justified if Γ also captures the penalty for non-negativity and DC-biasing [40]. In fact, it can be shown, that (9) can be derived from the bit error rate achieved by pulse amplitude modulation (PAM) or quadrature amplitude modulation (QAM), as a function of the constellation size (thus of the bit/s/Hz). By fixing the BER and absorbing the inverted error function as a constant into Γ, and by allowing an optimal constellation size for the given SNR, one arrives at an expression that relates the rate to the bandwidth and signal to noise ratio exactly as in (9), without relying on information theoretical capacity proofs [19]. $P_k(f)$ is the electrical power of the OFDM signals on the k-th independent channel modulated to the activated LEDs, which is subject to the power constraint

$$\sum_{k=1}^{K} \int_0^{f_{\max}} P_k(f) df = P_T, \tag{10}$$

where P_T is the total power available for transmission. Furthermore, we assume that P_T can meet the requirements of eye safety and practical illumination. The block diagram of the operation of practical power allocation is illustrated in Fig. 2. Note that the operation of power allocation for each LED is coordinated by a controller at the transmitter.

Subsequently, the overall achievable rate of the MIMO-OFDM VLC system over low-pass channels can be obtained by the sum of the achievable rates of all the independent data streams, expressed as

$$R = \sum_{k=1}^{K} \int_0^{f_{\max}} \log_2 \left(1 + \frac{\lambda_k P_k(f)}{a\Gamma N_0} 2^{-\frac{f}{f_c}}\right) df. \tag{11}$$

From (11), it can be further observed that the maximal achievable rate depends on the power allocation on each sub-carrier. Therefore, it merits further investigation upon the optimal power allocation to maximize the achievable rate with certain power constraint, as expressed by the optimization problem:

$$\max_{P_k(f)} \quad \sum_{k=1}^{K} \int_0^{f_{\max}} \log_2 \left(1 + \frac{\lambda_k P_k(f)}{a\Gamma N_0} 2^{-\frac{f}{f_c}}\right) df,$$
$$\text{s.t.} \quad P_k(f) \geq 0, \sum_{k=1}^{K} \int_0^{f_{\max}} P_k(f) df = P_T. \tag{12}$$

The above optimization problem is a convex with respect to the power variables since the associated constraints are affine. Moreover, the optical power constraints such as for eye safety can be also generalized with different P_T by exploring the electroluminescence mechanism in the LED from electrical power consumption to optical power output [19]. The power optimization for the proposed system is addressed in detail in the following sections.

III. Power Allocation Strategies

In this section, we propose 2D-WF strategy for power allocation and the corresponding achievable rate is analyzed. Other five conventional power allocation strategies are also investigated for comparison.

A. Water-Filling Power Allocation Strategy

If the transmitter and receiver both perfectly know the channel state information (CSI) in the OFDM systems, a well known power allocation optimization algorithm is water-filling (WF) [18], [20].

1) 2D-WF Power Allocation Strategy: We extend the frequency-domain 1D-WF into spatial domain in the MIMO-OFDM VLC system. For the proposed 2D-WF power allocation strategy, the maximal used bandwidth $f_{\max}$ varies for different sub-channels. Thus, we define the maximal used bandwidth of k-th sub-channel as $f_{\max_k}$. Following (12), based on Lagrangian algorithm, the power assigned to the k-th sub-channel at the f-th sub-carrier can be formulated as follows, and the detailed derivations are given in Appendix.

$$P_k(f) = [\mu - s_k(f)]^+, \tag{13}$$

where

$$s_k(f) = \frac{a\Gamma N_0}{\lambda_k} 2^{\frac{f}{f_c}} \tag{14}$$

is the inverse of the space-related channel gain to noise ratio and $[x]^+ = x$, if $x > 0$, and $[x]^+ = 0$, if $x \leq 0$. Since singular values λ_k result from the SVD operation of the channel matrix $\mathbf{H}(0)$ that is determined by the spacial locations through Eq. (4), the proposed 2D-WF algorithm allocates the power in space domain based on singular values λ_k. The coefficient $\mu = 1/(2\ln(2)L)$ is a constant determined by the power constraint:

$$\sum_{k=1}^{K} \int_0^{f_{\max_k}} [\mu - s_k(f)]^+ df = P_T. \tag{15}$$

For the proposed 2D-WF power allocation strategy, as we can see from Fig. 3 that $P_k(f) > 0$ only for $f \in [0, f_{\max_k}]$, we have

Authorized licensed use limited to: CHONGQING UNIVERSITY. Downloaded on July 16,2022 at 07:24:30 UTC from IEEE Xplore. Restrictions apply.

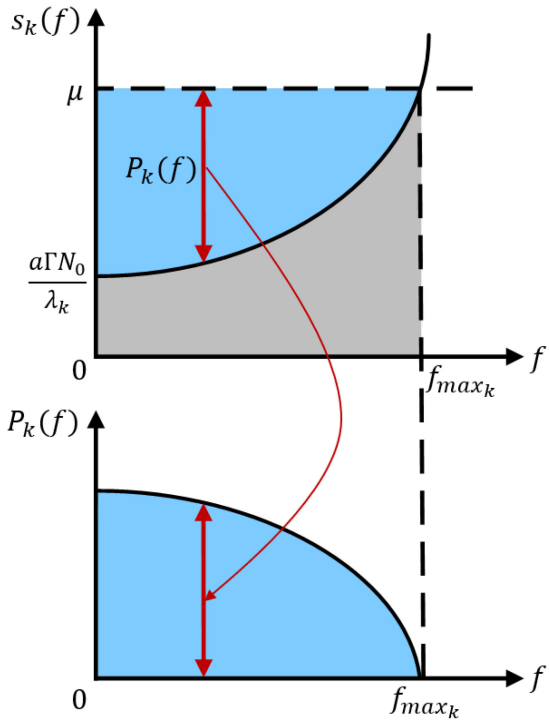

Fig. 3. Illustration of $s_k(f)$ and $P_k(f)$. .

$\mu = s_k(f_{\max_k})$. Thus, the optimal value of $P_k(f)$ becomes

$$P_k(f) = s_k(f_{\max_k}) - s_k(f) = \frac{a\Gamma N_0}{\lambda_k}\left(2^{\frac{f_{\max_k}}{f_c}} - 2^{\frac{f}{f_c}}\right), \tag{16}$$

and thus, by inserting (16) into (11), the overall maximum achievable rate of MIMO-OFDM VLC systems over the low-pass channels with the proposed 2D-WF power allocation strategy can be expressed as

$$R_w = \sum_{k=1}^{K}\int_0^{f_{\max_k}}\left(\frac{f_{\max_k} - f}{f_c}\right)df = \frac{1}{2f_c}\sum_{k=1}^{K} f_{\max_k}^2. \tag{17}$$

For a fair performance comparison, we define the normalized overall achievable rate to the 3 dB bandwidth f_c of the LED as

$$\Re_w = \frac{R_w}{f_c} = \frac{1}{2}\sum_{k=1}^{K} v_{\max_k}^2, \tag{18}$$

where $v_{\max_k} = f_{\max_k}/f_c$ is the normalized bandwidth of the k-th sub-channel related to the frequency f_c.

Without loss generality, we sort the used set $\{\lambda_k\}$, letting $\lambda_k \geq \lambda_{k+1}$, so λ_K is the minimal used value of set $\{\lambda_k\}$. Since $\mu = s_1(f_{\max_1}) = \cdots = s_k(f_{\max_k}) = \cdots = s_K(f_{\max_K})$, thus, following (14) we can calculate $v_{\max_k}, k = 1, 2, \ldots, K-1$ by

$$v_{\max_k} = v_{\max_K} + \log_2\left(\frac{\lambda_k}{\lambda_K}\right). \tag{19}$$

Then, there is only one variable $v_{\max_K}$, i.e., the normalized bandwidth of the sub-channel with the minimal singular value. In consequence, we can rewrite (18) as

$$\Re_w = \frac{1}{2}\sum_{k=1}^{K}\left(v_{\max_K} + \log_2\left(\frac{\lambda_k}{\lambda_K}\right)\right)^2. \tag{20}$$

In this work, the transmit SNRs and the received SNRs of different sub-channels might be different due to different power allocation and different transmission paths. As a result, it is difficult to use the transmit SNRs or received SNRs of each sub-channel as the metric to evaluate the performance of MIMO-OFDM VLC systems over low-pass channels. For a fair performance comparison, we define the total transmit SNR, or in fact the link power budget, to the 3 dB bandwidth f_c of the LED, as

$$\gamma = \frac{P_T}{N_0 f_c}.$$

Then, by inserting (16) in (15), it is possible to rewrite (15) as

$$\sum_{k=1}^{K}\frac{a\Gamma}{\lambda_k \ln 2}\left(2^{v_{\max_k}}\left(v_{\max_k}\ln 2 - 1\right) + 1\right) = \gamma, \tag{21}$$

where $v_{\max_k}$ is defined by (19).

Since some LEDs might be not used for communication due to the limited power budget, it is impossible to directly solve the above equations. Next, we propose an algorithm for obtaining the maximal achievable rate of MIMO-OFDM VLC systems over the low-pass channels with the proposed 2D-WF power allocation strategy.

As we can see from the Algorithm 1, firstly, we set the iteration count t to 1 and compute $v_{\max_{K-t+1}}$ by solving the following equation:

$$\sum_{k=1}^{K-t+1}\frac{a\Gamma}{\lambda_k \ln 2}\left(2^{v_{\max_k}}\left(v_{\max_k}\ln 2 - 1\right) + 1\right) = \gamma, \tag{22}$$

where

$$v_{\max_k} = v_{\max_{K-t+1}} + \log_2\left(\frac{\lambda_k}{\lambda_{K-t+1}}\right). \tag{23}$$

Secondly, if the obtained optimal normalized modulation bandwidth has the negative value (i.e., if $v_{\max_{K-t+1}} < 0$), discard that sub-channel with the minimal eigenvalue λ_{K-t+1} and rerun the algorithm with the iteration count t incremented by 1. It should be noted that if the sub-channel is discarded, the corresponding LED will be deactivated for communication and only the DC bias is applied to maintain its illumination function. Then, by repeating the first step and the second step until the optimal normalized modulation bandwidth has the non-negative value.

Lastly, we can compute the maximal achievable rate $\Re_w$ by the following equation:

$$\Re_w = \frac{1}{2}\sum_{k=1}^{K-t+1}\left(v_{\max_{K-t+1}} + \log_2\left(\frac{\lambda_k}{\lambda_{K-t+1}}\right)\right)^2. \tag{24}$$

To compare our proposed 2D-WF power allocation strategy with the conventional WF algorithm, two conventional 1D-WF

Authorized licensed use limited to: CHONGQING UNIVERSITY. Downloaded on July 16,2022 at 07:24:30 UTC from IEEE Xplore. Restrictions apply.

Algorithm 1: Algorithm for the Proposed 2D-WF Power Allocation Strategy.

Input: Link power budget: γ; Eigenvalue set: $\{\lambda_k\}$; Rank of channel matrix: K.
Output: The maximal achievable rate $\mathfrak{R}_w$.

```
Initialize t = 1;
Compute v_max_{K-t+1} by solving (22) and (23);
while v_max_{K-t+1} < 0 do
    v_max_{K-t+1} = 0;
    if t ≤ K then
        t=t+1;
        Update v_max_{K-t+1} by solving (22) and (23);
    end
end
Compute ℜ_w by solving (23) and (24).
```

algorithms including only space domain WF [30] and only frequency domain WF [28] are introduced.

2) WF Power Allocation Only Over Space Domain: For the WF algorithm only over space domain (1D-WFS), the modulation bandwidths of all sub-channel are equal. It allocates uniform power for different frequencies, i.e., constant power spectrum in each LED sub-channel, hence, the power assigned to the k-th sub-channel at the f-th sub-carrier can be written as

$$P_k(f) = \frac{P_k}{f_{\max}}, \tag{25}$$

where P_k is the power assigned to the k-th sub-channel, and can be calculated by

$$P_k = \left[\varepsilon - \frac{a\Gamma N_0}{\lambda_k}\right]^+, \tag{26}$$

where ε indicates the constant power level in space domain. P_k is subject to the power constraint:

$$\sum_{k=1}^{K} P_k = P_T. \tag{27}$$

Thus, the maximal achievable rate of 1D-WFS can be expressed as

$$\mathfrak{R}_{ws} = \sum_{k=1}^{K} \int_0^{v_{\max}} \log_2\left(1 + \frac{\lambda_k P_k}{a\Gamma N_0 f_{\max}} 2^{-v}\right) dv. \tag{28}$$

3) WF Power Allocation Only Over Frequency Domain: The power assigned to the k-th sub-channel at the f-th sub-carrier for WF power allocation only over frequency domain (1D-WFF) can be expressed as

$$P_k(f) = [\mu_f - s(f)]^+, \tag{29}$$

where

$$s(f) = s(0)2^{\frac{f}{f_c}}. \tag{30}$$

The power constraint:

$$\int_0^{f_{\max}} \left[\mu_f - s(0)2^{\frac{f}{f_c}}\right]^+ df = \frac{P_T}{K}. \tag{31}$$

Since $P_k(f) > 0$ only for $f \in [0, f_{\max}]$, we have $\mu_f = s(f_{\max}) = s(0)2^{v_{\max}}$.

So,

$$s(0) = \frac{P_T \ln 2}{K f_c((v_{\max}\ln 2 - 1)2^{v_{\max}} + 1)}, \tag{32}$$

$$P_k(f) = \frac{P_T \ln 2\left(2^{v_{\max}} - 2^{\frac{f}{f_c}}\right)}{K f_c((v_{\max}\ln 2 - 1)2^{v_{\max}} + 1)}. \tag{33}$$

By solving the above equation, we can get the optimal modulation bandwidth $v_{\max}$, thus, we can obtain the maximal achievable rate of 1D-WFF:

$$\mathfrak{R}_{wf} = \sum_{k=1}^{K} \int_0^{v_{\max}} \log_2\left(1 + \frac{\lambda_k \gamma \ln 2\,(2^{v_{\max}-v} - 1)}{a\Gamma K((v_{\max}\ln 2 - 1)2^{v_{\max}} + 1)}\right) dv. \tag{34}$$

Fig. 4 illustrates different WF power allocation strategies over equal low-pass channels both in space and frequency domains, i.e., the proposed 2D-WF in frequency (a) and space (d) domain, only space 1D-WFS in space (b) and frequency (e) domain, and only frequency 1D-WFF in frequency (c) and space (f) domain. As we can see, 2D-WF allocates different powers according to the low-pass LED channel and the corresponding power in each LED channel also varies (as indicated by power factor ε_k), which is in contrast to 1D-WFS where the corresponding power in each LED channel remains constant. 1D-WFS allocates different powers in each LED but it allocates uniform power spectrum (power in every frequency bin) in each LED channel.

4) WF Power Allocation Without Low-Pass Effect: The low-pass effect has been overlooked in most of the reported publications, as in Table I. In this case, the normalized overall achievable rate of the MIMO-OFDM VLC system with WF power allocation strategy in space domain can be calculated by

$$\mathfrak{R}_{n,w} = v_{\max} \sum_{k=1}^{K} \log_2\left[\frac{\lambda_k}{a\Gamma N_0}\delta\right]^+, \tag{35}$$

where the coefficient δ is a constant and determined by the power constraint

$$\sum_{k=1}^{K} f_{\max}\left[\delta - \frac{a\Gamma N_0}{\lambda_k}\right]^+ = P_T. \tag{36}$$

The achievable rate without low-pass effect in (35) represents an ideal system and deviates from the reality. But as a benchmark, it can be used to quantify the impact of low-pass effect on the achievable rate as presented in Section IV. Other three conventional power allocation algorithms, including UF, PE and BF power allocation strategies are introduced for comparison with our proposed 2D-WF power allocation strategy.

B. Uniform Power Allocation Strategy

By using the SVD theorem, the MIMO channels are decomposed into statistically independent equivalent sub-channel, and by OFDM modulation, each LED transmits statistically independent data symbols on multiple sub-carriers. At the transmitter, the most simple strategy is to assign equal transmit energy to each sub-channel of each sub-carrier. This UF power allocation

Authorized licensed use limited to: CHONGQING UNIVERSITY. Downloaded on July 16,2022 at 07:24:30 UTC from IEEE Xplore. Restrictions apply.

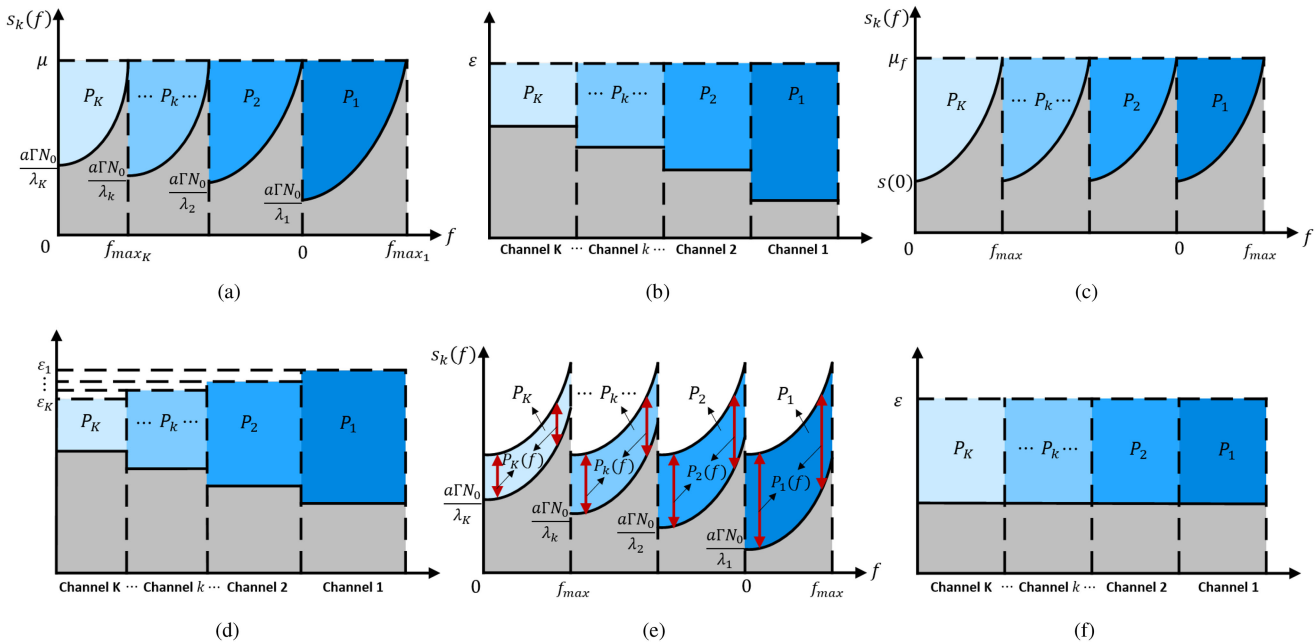

Fig. 4. Illustration of WF power allocation strategy over equal low-pass channels in (a) space-frequency domain, (b) only space domain, (c) only frequency domain. (d) the space domain perspective of '(a),' (e) the frequency domain perspective of '(b),' (f) the space domain perspective of '(c)'.

strategy appears to be relevant to current standardization, in particular ITU g.9991 [41]. Thus, the power assigned to the k-th sub-channel at the f-th sub-carrier can be formulated as follows

$$P_k(f) = \frac{P_T}{K f_{\max}}, k = 1, 2, \ldots, K. \tag{37}$$

Then, the overall achievable rate of the MIMO-OFDM VLC system over the equal low-pass channels with UF power allocation strategy can be computed by

$$R_u = \sum_{k=1}^{K} \int_0^{f_{\max}} \log_2 \left(1 + \frac{\lambda_k P_T}{a\Gamma N_0 K f_{\max}} 2^{-\frac{f}{f_c}}\right) df. \tag{38}$$

For a fair performance comparison, we define the normalized overall achievable rate as

$$\begin{aligned}\Re_u = \frac{R_u}{f_c} &= \frac{1}{f_c} \sum_{k=1}^{K} \int_0^{f_{\max}} \log_2 \left(1 + \eta_k 2^{-\frac{f}{f_c}}\right) df \\ &= \sum_{k=1}^{K} \int_0^{v_{\max}} \log_2 \left(1 + \eta_k 2^{-v}\right) dv, \end{aligned} \tag{39}$$

where

$$\eta_k = \frac{\lambda_k \gamma}{a\Gamma K v_{\max}}$$

and $v_{\max} = f_{\max}/f_c$ is the normalized bandwidth related to the frequency f_c.

Using $\log_2(x) = \ln(x)/\ln(2)$ and employing the u-substitution method we can rewrite (39) as

$$\Re_u = \frac{1}{(\ln 2)^2} \sum_{k=1}^{K} \left[Li_2\left(-\eta_k 2^{-v_{\max}}\right) - Li_2\left(-\eta_k\right)\right], \tag{40}$$

where $Li_2(x)$ is the Spence's function defined as [19]

$$Li_2(x) = \int_0^x \frac{\ln(1-u)}{-u} du. \tag{41}$$

Therefore, in this case, the normalized optimum modulation bandwidth can then be found to maximize the normalized overall achievable rate by calculating $d\Re_u/dv_{\max} = 0$, which can be obtained as

$$\sum_{k=1}^{K} v_{\max} \ln(2) \log_2\left(1+\eta_k 2^{-v_{\max}}\right) = \sum_{k=1}^{K} \int_0^{v_{\max}} \left(\frac{\eta_k}{2^v + \eta_k}\right) dv. \tag{42}$$

If we not consider the low-pass effect, the normalized overall achievable rate of the MIMO-OFDM VLC system with UF power allocation strategy can be calculated by

$$\Re_{n,u} = v_{\max} \sum_{k=1}^{K} \log_2\left(1 + \eta_k\right). \tag{43}$$

C. Per-Emphasis Power Allocation Strategy

The followings discuss the overall maximum achievable rate of a OFDM-based MIMO-VLC system with a PE power allocation algorithm. PE algorithm is aimed at eliminating the low-pass effect at the transmitter, i.e., transmits more power at high frequency. Hence, the power assigned to each sub-channel with a PE strategy can be written as [19]

$$P_k(f) = P_0 |h(f)|^{-2} = b \frac{P_T}{K f_{\max}} 2^{\frac{f}{f_c}}, \tag{44}$$

where

$$P_0 = P_k(0) = b \frac{P_T}{K f_{\max}}$$

Authorized licensed use limited to: CHONGQING UNIVERSITY. Downloaded on July 16,2022 at 07:24:30 UTC from IEEE Xplore. Restrictions apply.

denotes a power back-off b of UF power allocation and b is determined by the power constraint of transmitter, i.e.,

$$\sum_{k=1}^{K}\int_{0}^{f_{\max}} b\frac{P_T}{Kf_{\max}}2^{\frac{f}{f_c}}df = P_T. \tag{45}$$

By solving (45), b can be expressed as

$$b = \frac{v_{\max}\ln 2}{2^{v_{\max}}-1}. \tag{46}$$

So based on above expressions, by inserting (44) and (46) in (11), the overall maximum achievable rate of MIMO-OFDM VLC system over the equal low-pass channels with the PE power allocation algorithm can be written as

$$R_p = \sum_{k=1}^{K}\int_{0}^{f_{\max}} \log_2\left(1+\frac{v_{\max}\ln 2}{2^{v_{\max}}-1}\frac{\lambda_k P_T}{a\Gamma N_0 K f_{\max}}\right)df. \tag{47}$$

Thus, as same as WF power allocation algorithm and UF power allocation algorithm, we define the normalized overall achievable rate of MIMO-OFDM VLC system over the equal low-pass channels with PE power allocation algorithm as

$$\Re_p = \frac{R_p}{f_c} = v_{\max}\sum_{k=1}^{K}\log_2\left(1+\frac{\ln(2)\lambda_k\gamma}{a\Gamma K(2^{v_{\max}}-1)}\right). \tag{48}$$

For this case, the normalized optimum modulation bandwidth can then be found to maximize the normalized overall achievable rate of PE algorithm by calculating $d\Re_p/dv_{\max}=0$. Thus, we can get the relationship between the normalized optimum modulation bandwidth and the link budget:

$$\sum_{k=1}^{K}\log_2\left(1+\frac{\ln(2)\lambda_k\gamma}{a\Gamma K(2^{v_{\max}}-1)}\right) = \sum_{k=1}^{K}\frac{\ln(2)\lambda_k\gamma v_{\max}2^{v_{\max}}}{a\Gamma K(2^{v_{\max}}-1)+\ln(2)\lambda_k\gamma}. \tag{49}$$

In the following, we address the last power power allocation strategy, namely BF power allocation algorithm.

D. Beamforming Power Allocation Strategy

If the quality of MIMO channel is very bad, we should use the best parallel sub-channel. Therefore, we consider a particular form of WF power allocation strategy, i.e., BF power allocation strategy in which information is only transmitted over a single eigenmode, i.e., the one with the largest eigenvalue [30].

Without loss of generality, we assume that λ_1 is the largest eigenvalue. Following (18), the normalized overall achievable rate of the MIMO-OFDM VLC system over the equal low-pass channels with BF power allocation strategy can be calculated by

$$\Re_b = \frac{1}{2}v_{\max_1}^2, \tag{50}$$

and follow (21), we can get the power constraint for single-mode allocation as

$$\frac{a\Gamma}{\lambda_1\ln 2}\left(2^{v_{\max_1}}\left(v_{\max_1}\ln 2-1\right)+1\right)=\gamma. \tag{51}$$

TABLE II
POWER ALLOCATION STRATEGY

Strategy	Space/Frequency domain	Problem
WF	S&F	Algorithm 1
	S	max Eq.(28)
	F	max Eq.(34)
UF	S&F	max Eq.(40) s.t. Eq.(42)
PE	S&F	max Eq.(48) s.t. Eq.(49)
BF	S&F	max Eq.(50) s.t. Eq.(51)

TABLE III
SIMULATION PARAMETERS

Parameter	Value
Room dimension	5 m × 5 m × 3 m
Height of receiving plane	0.85 m
Semiangle at half power of LED ($\Phi_{\frac{1}{2}}$)	70°
FOV Semiangle ($\Psi_{\frac{1}{2}}$)	70°
Responsivity of PD (ρ)	0.53 A/W
Active area of PD (A)	1 cm^2
Modulation gap (Γ)	6.06 dB
Elevation angle (β)	15°
3dB cut-off frequency (f_c)	10 MHz
Locations of the 2 × 2 LEDs (m)	(-1,0,3),(1,0,3)
Locations of user in case 1 (m)	(0,0,0.85),(0.2,0,0.85)
Azimuth angle of user in case 1 (α)	180°, 0°
Locations of user in case 2 (m)	(-2.5,-2.5,0.85),(-2.3,-2.5,0.85)
Azimuth angle of user in case 2 (α)	75°, 15°
Locations of the 4 × 4 LEDs (m)	(-1, 1,3),(1, 1,3) (1,-1,3),(-1,-1,3)
Locations of the 4 × 4 PDs (m)	(0.01,0.2,0.85),(0.21,0.2,0.85) (0.21, 0 ,0.85),(0.01, 0 ,0.85)
Azimuth angle of the 4 × 4 PDs (α)	135°, 45°, 315°, 225°

If the low-pass effect was not considered, the normalized overall achievable rate of the MIMO-OFDM VLC system with BF power allocation strategy can be calculated by

$$\Re_{n,b} = v_{\max}\log_2\left(1+\frac{\lambda_1\gamma}{a\Gamma v_{\max}}\right). \tag{52}$$

Based on above discussions, we have derived expressions on the achievable rate with respect to the modulation bandwidth and link power budget in the MIMO-OFDM VLC systems, as summarized in Table II. In particular, we take into consideration the effect of low-pass channel in all power allocation strategies.

IV. RESULTS

In this section, we evaluate and compare the performance of a MIMO-OFDM VLC system over low-pass channels with different power allocation strategies in a typical indoor environment. We assume that the LED array is in the center of a room with the coordinate (0,0,0). The geometric setup and the Cartesian coordinate system of a VLC system are shown in Fig. 5(a), and the top view of the 2 × 2 and 4 × 4 MIMO-OFDM VLC system in Fig. 5(b) and (c), respectively. The simulation parameters are list in Table III. In particular, we apply different azimuth angles of PDs in ADR to reduce the channel correlation. Based on this setup, the DC channel gain matrices of the proposed system are given by followings.

Authorized licensed use limited to: CHONGQING UNIVERSITY. Downloaded on July 16,2022 at 07:24:30 UTC from IEEE Xplore. Restrictions apply.

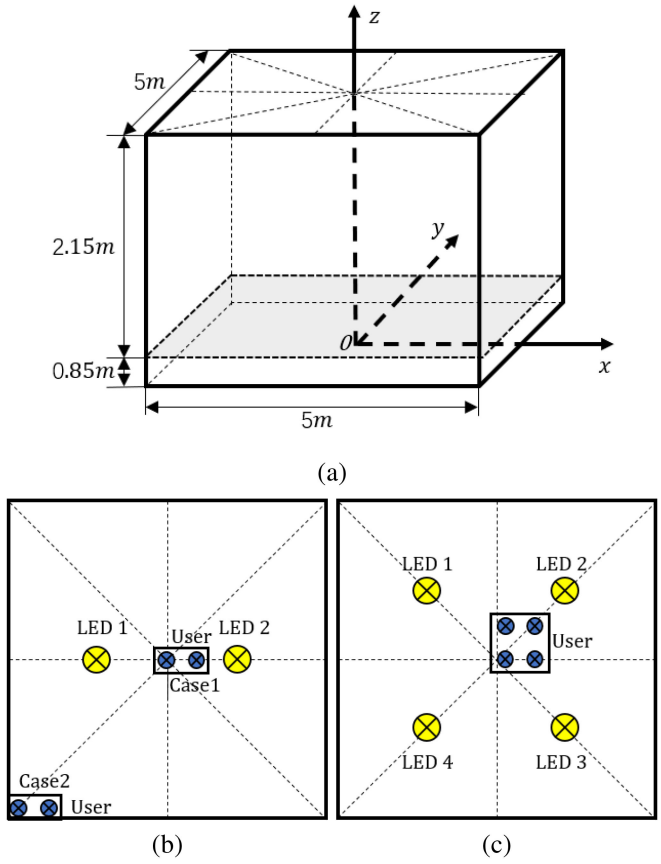

Fig. 5. Illustration of (a) geometric setup and the Cartesian coordinate system of VLC system and top view of the (b) 2×2 and (c) 4×4 MIMO-VLC system.

User in case 1:

$$\mathbf{H}_1(0) = 10^{-6}\begin{bmatrix} 2.283 & 1.777 \\ 1.505 & 2.519 \end{bmatrix}. \tag{53}$$

User in case 2:

$$\mathbf{H}_2(0) = 10^{-7}\begin{bmatrix} 5.843 & 2.180 \\ 5.801 & 2.545 \end{bmatrix}. \tag{54}$$

4×4:

$$\mathbf{H}_{4\times4}(0) = 10^{-6}\begin{bmatrix} 1.923 & 1.650 & 1.087 & 1.311 \\ 1.411 & 2.219 & 1.427 & 0.940 \\ 1.072 & 1.645 & 1.940 & 1.307 \\ 1.499 & 1.249 & 1.516 & 1.764 \end{bmatrix}. \tag{55}$$

The condition number of the channel matrix (53)–(55) are 28, 1260, and 5066 respectively. As we can see from (53) and (54), the channel coefficients are in the order of 10^{-6} and 10^{-7}. This means there are electrical path loss of about 120 dB and 140 dB [23]. Thus, for a fair comparison in this work, we set the same link power budget (i.e., total transmit SNR) in the range between 120 dB to 160 dB and 140 dB to 160 dB for our numerical simulations.

A. Water-Filling Power Allocation Strategy

Firstly, we compare the achievable rate of the proposed 2D-WF power allocation strategy with two conventional 1D-WF

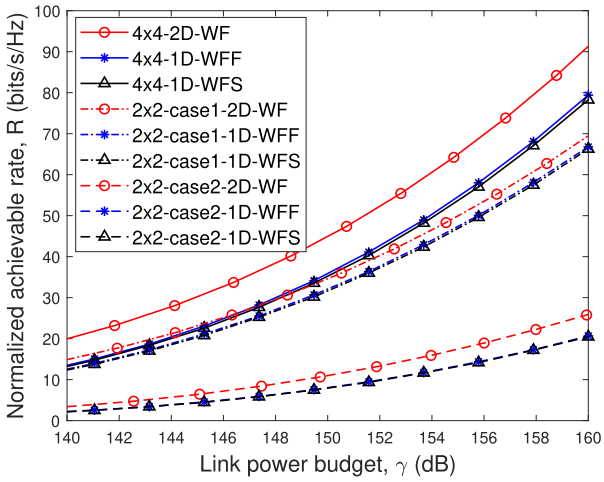

Fig. 6. Comparison of WF power allocation strategy over space-frequency domain, only space domain and only frequency domain for two 2×2 MIMO-OFDM VLC system and a 4×4 MIMO-OFDM VLC system with low-pass effect.

power allocation strategies for two 2×2 cases and a 4×4 case of MIMO-OFDM VLC system with low-pass effect. As we can see from Fig. 6, the proposed 2D-WF power allocation strategy outperforms both 1D-WFS and 1D-WFF in all cases. Furthermore, with the increase of the number of transmitters and receivers, the performance of the proposed 2D-WF power allocation strategy is significantly improved. And in the small link power budget region of case 1, the 2×2 MIMO-OFDM VLC system with 2D-WF outperforms the 4×4 MIMO-OFDM VLC system with 1D-WFF or 1D-WFS. Although the achievable rate of 1D-WFS is close to 1D-WFF in case 2, the 1D-WFF always outperforms the 1D-WFS in all cases. In particular, the achievable rate increment by the proposed 2D-WF power allocation strategy in case 1 is less than that in case 2 of the 2×2 MIMO-OFDM VLC system, which is due to the condition number of $\mathbf{H}_1(0)$ is far smaller than that of $\mathbf{H}_2(0)$, i.e., the channel correlation of case 1 is far larger than that of case 2 such that the spatial diversity is limited for MIMO-OFDM system in case 1.

B. Comparison of Different Power Allocation Strategies

In this section, we investigate the achievable rates of the MIMO-OFDM VLC system over low-pass channels with four different power allocation strategies, namely 2D-WF, UF, PE and BF power allocation.

To get a clear view of the change in modulation bandwidth, we consider the case 1 in the 2×2 MIMO-OFDM VLC system. Fig. 7 illustrates the normalized achievable rate versus the normalized modulation bandwidth $v_{\max}$ with three given link power budget, 140 dB, 150 dB, 160 dB. The figure shows that an optimal $v_{\max}$ exists for a given link power budget for UF power allocation strategy and PE power allocation strategy. However, 2D-WF power allocation strategy will not show this property since it already used the optimal bandwidth for each

Authorized licensed use limited to: CHONGQING UNIVERSITY. Downloaded on July 16,2022 at 07:24:30 UTC from IEEE Xplore. Restrictions apply.

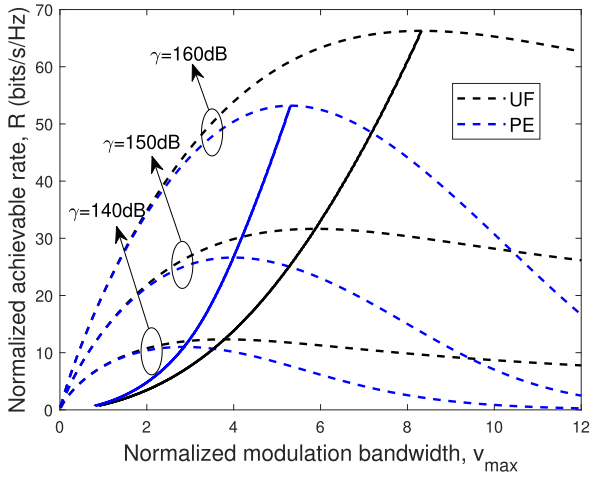

Fig. 7. Normalized achievable rate (dashed curves) versus normalized modulation bandwidth $v_{\max}$ with different link power budget γ and maximal normalized achievable rate (solid curves) versus optimal normalized modulation bandwidth $v_{\max}$ for a 2×2 MIMO-OFDM VLC system over low-pass channels with UF power allocation strategy (black curves) and PE power allocation strategy (blue curves) in case 1, respectively.

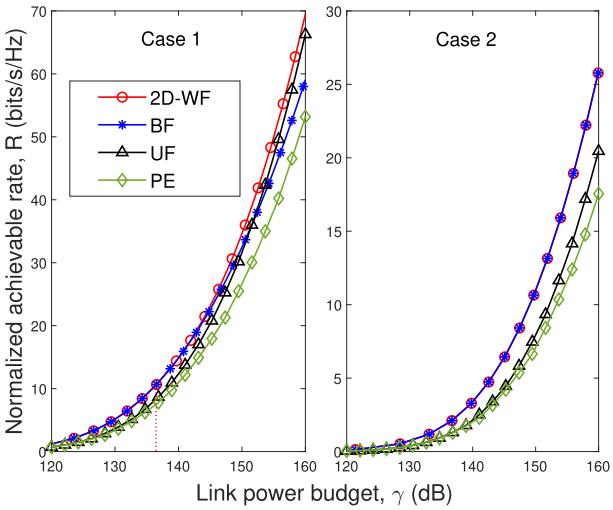

Fig. 8. Normalized achievable rate versus the link power budget γ for a 2×2 MIMO-OFDM VLC system over low-pass channels with four different power allocation strategies in case 1 and case 2.

sub-channel, as indicated in (18). Then, we investigate the performance comparison for UF and PE power allocation strategy by using the optimal normalized modulation bandwidth $v_{\max}$.

Fig. 8 illustrates the normalized achievable rate versus the link power budget γ for a 2×2 MIMO-OFDM VLC system over low-pass channels with four different power allocation strategies in case 1 and case 2. It can be observed from Fig. 8 that the 2D-WF power allocation strategy can achieve the highest rate, while the PE power allocation strategy has the lowest in case 1. It is expected that higher link power budget γ leads to better achievable rate. Interestingly, the BF power allocation strategy does not always outperform the UF power allocation strategy in case 1. When the link power budget becomes relatively large, the

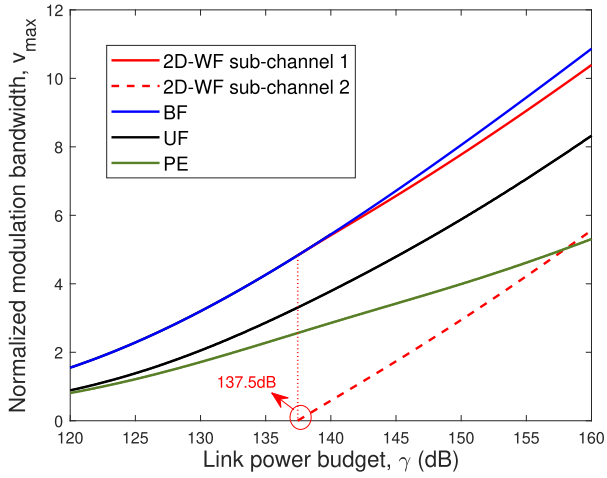

Fig. 9. Optimal normalized modulation bandwidth $v_{\max}$ versus the link power budget γ for a 2×2 MIMO-OFDM VLC system over low-pass channels with four different power allocation strategies in case 1.

UF power allocation strategy outperforms the BF power allocation strategy. In case 2, the curve of 2D-WF overlaps with that of BF, which means the 2D-WF discards the bad sub-channel, and only transmits information over the good sub-channel, i.e., 2D-WF becomes BF. This is because the condition number of $\mathbf{H}_2(0)$ is very large. This also indicates the robustness of our proposed 2D-WF algorithm which can achieve the optimal power allocation according to the channel condition.

To further explain the phenomenon of case 1 in Fig. 8, where the curve of 2D-WF overlaps with that of BF in the region of small link power budget, we illustrate the optimal normalized modulation bandwidth $v_{\max}$ versus the link power budget γ in Fig. 9. As we can observe that when the link power budget is relatively small, the optimal normalized modulation bandwidth of 2D-WF power allocation strategy is the same as BF power allocation strategy. This means the quality of MIMO channel is bad, and the 2D-WF power allocation strategy only transmits information over the sub-channel with the largest eigenvalue, i.e., when the link power budget is lower than 137.5 dB, the 2D-WF becomes the BF. Thus, our proposed 2D-WF algorithm can achieve the adaptive power allocation according to the channel condition and the link power budget.

C. *Without Low-Pass Effect*

Moreover, it can be observed by the comparison with Fig. 8 and Fig. 10, that the achievable rate of the MIMO-OFDM system without low-pass effect is much higher than that with low-pass effect, i.e., the low-pass channels inevitably affect the data rate of VLC systems. In this case, since there is no freedom in frequency domain for WF, only 1D-WFS is applied. In fact, the low-pass nature is an essential aspect that has to be considered by system designers, while, unfortunately, barely be paid attention. In case 1 of Fig. 10, it is possible to observe that, the 1D-WFS power allocation strategy achieves the highest rate over both small and large link power budget regions, and outperforms the UF power allocation strategy in the small link

Authorized licensed use limited to: CHONGQING UNIVERSITY. Downloaded on July 16,2022 at 07:24:30 UTC from IEEE Xplore. Restrictions apply.

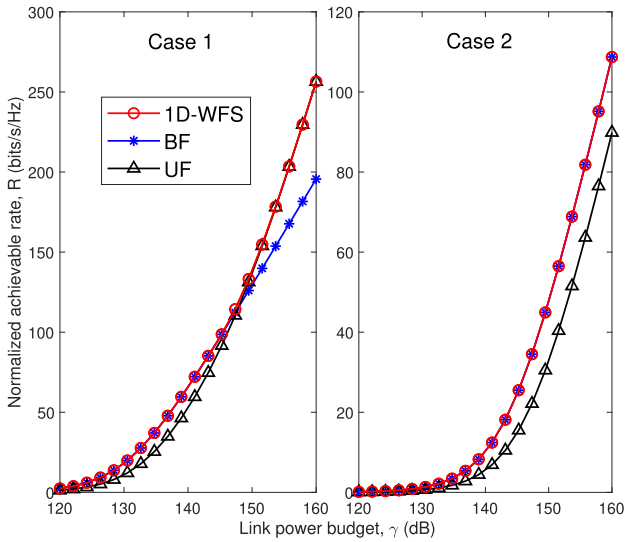

Fig. 10. Normalized achievable rate versus link budget γ for a 2×2 MIMO-OFDM VLC system without low-pass effect in case 1 and case 2.

power budget region, but when the link power budget becomes relatively large the UF power allocation strategy closely matches the 1D-WFS power allocation strategy. Moreover, when the link power budget is more than a threshold value, the UF power allocation strategy outperforms the BF power allocation strategy. Interestingly, when the link power budget is lower than a other threshold value, the 1D-WFS power allocation strategy becomes the BF power allocation strategy, as we observed in 2D-WF case. This is further confirmed in case 2, where the performance of 1D-WFS matches with that of BF over both small and large link power budget regions, which means the 1D-WFS only transmits information over the good sub-channel.

V. Conclusion

We introduced a model for describing the throughput of MIMO-OFDM VLC systems over low-pass LED channels in an indoor environment and we pointed out the disruptive effect of low-pass behavior on the achievable rate of the MIMO-OFDM system. To the best of our knowledge, low-pass MIMO-OFDM VLC with a matrix channel decomposition has not extensively been treated theoretically in literature. Moreover, we investigate six power allocation strategies over space and (or) frequency domain for the proposed system, including 2D-WF power allocation, 1D-WFS and 1D-WFF power allocation, UF power allocation, PE power allocation and BF power allocation. In this paper, for the first time, we propose the 2D-WF power allocation strategy over both space domain and frequency domain for the MIMO-OFDM VLC system over low-pass channels. Simulation results show that the throughput of a MIMO-OFDM VLC system over low-pass channels with the proposed 2D-WF power allocation strategy is greater than that of the rest of reported power allocation algorithms. The low-pass nature in practical MIMO-OFDM VLC channels inevitably affects the data rate and quality of service in VLC systems, especially in a massive LED luminaires scenario, which should be further investigated in future research.

Appendix A
Derivations for 2D-WF Power Allocation

Firstly, we introduce a Lagrange function:

$$F(P_k(f), L) = \sum_{k=1}^{K} \int_0^{f_{\max_k}} \log_2 \left(1 + \frac{\lambda_k P_k(f)}{a\Gamma N_0} 2^{-\frac{f}{f_c}}\right) df + L\left(P_T - \sum_{k=1}^{K} \int_0^{f_{\max_k}} P_k(f) df\right), \quad (56)$$

where L is a constant called the Lagrange multiplier.

Following (56), the choice of $P_k(f)$ that maximizes the Lagrange function F can be determined by maximizing the integral:

$$\sum_{k=1}^{K} \int_0^{f_{\max_k}} \left(\log_2 \left(1 + \frac{\lambda_k P_k(f)}{a\Gamma N_0} 2^{-\frac{f}{f_c}}\right) - L P_k(f)\right) df. \quad (57)$$

Moreover, by the properties of definite integrals, the choice of $P_k(f)$ that maximizes the integral (57) can be determined by maximizing the integrand:

$$J(P_k(f), L) = \sum_{k=1}^{K} \left(\log_2 \left(1 + \frac{\lambda_k P_k(f)}{a\Gamma N_0} 2^{-\frac{f}{f_c}}\right) - L P_k(f)\right). \quad (58)$$

Next, we take the partial derivative of J with respect to the variables that we are attempting to optimize (i.e., $\{P_k(f)\}$) and set them equal to zero, i.e.,

$$\frac{\partial J(P_k(f), L)}{\partial P_k(f)} = 0,$$

which we can get the optimal value of $P_k(f)$, and can be expressed as

$$P_k(f) = \left[\mu - \frac{a\Gamma N_0}{\lambda_k} 2^{\frac{f}{f_c}}\right]^+, \quad (59)$$

where $\mu = 1/(2\ln(2)L)$ is a constant determined by the power constraint.

References

[1] T. Komine and M. Nakagawa, "Fundamental analysis for visible-light communication system using LED lights," *IEEE Trans. Consum. Electron.*, vol. 50, no. 1, pp. 100–107, Feb. 2004.

[2] P. Yang, Y. Xiao, M. Xiao, and S. Li, "6G wireless communications: Vision and potential techniques," *IEEE Netw.*, vol. 33, no. 4, pp. 70–75, Jul./Aug. 2019.

[3] X. Deng *et al.*, "Mitigating LED nonlinearity to enhance visible light communications," *IEEE Trans. Commun.*, vol. 66, no. 11, pp. 5593–5607, Nov. 2018.

[4] S. Mardani, A. Khalid, F. M. Willems, and J.-P. Linnartz, "Effect of blue filter on the SNR and data rate for indoor visible light communication system," in *Proc. Eur. Conf. Opt. Commun.*, 2017, pp. 1–3.

[5] H. Yang, J. W. Bergmans, T. C. Schenk, J.-P. M. Linnartz, and R. Rietman, "Uniform illumination rendering using an array of LEDs: A signal processing perspective," *IEEE Trans. Signal Process.*, vol. 57, no. 3, pp. 1044–1057, Mar. 2009.

Authorized licensed use limited to: CHONGQING UNIVERSITY. Downloaded on July 16,2022 at 07:24:30 UTC from IEEE Xplore. Restrictions apply.

[6] D. O'Brien, "Multi-input multi-output (MIMO) indoor optical wireless communications," in *Proc. 43rd Asilomar Conf. Rec. Signals, Syst. Comput.*, 2009, pp. 1636–1639.
[7] H. B. Eldeeb, S. M. Mana, V. Jungnickel, P. Hellwig, J. Hilt, and M. Uysal, "Distributed MIMO for Li-Fi: Channel measurements, ray tracing and throughput analysis," *IEEE Photon. Technol. Lett.*, vol. 33, no. 16, pp. 916–919, Aug. 2021.
[8] L. Zeng *et al.*, "High data rate multiple input multiple output (MIMO) optical wireless communications using white LED lighting," *IEEE J. Sel. Areas Commun.*, vol. 27, no. 9, pp. 1654–1662, Dec. 2009.
[9] C. Chen and W.-D. Zhong, "Hybrid space-frequency domain pre-equalization for DC-biased optical orthogonal frequency division multiplexing based imaging multiple-input multiple-output visible light communication systems," *Opt. Eng.*, vol. 56, no. 3, 2017, Art. no. 036102.
[10] A. H. Azhar, T. Tran, and D. O'Brien, "Demonstration of high-speed data transmission using MIMO-OFDM visible light communications," in *Proc. IEEE Globecom Workshops*, 2010, pp. 1052–1056.
[11] A. H. Azhar, T. A. Tran, and D. O'Brien, "A gigabit/s indoor wireless transmission using MIMO-OFDM visible-light communications," *IEEE Photon. Technol. Lett.*, vol. 25, no. 2, pp. 171–174, Jan. 2013.
[12] J.-P. M. Linnartz, X. Deng, A. Alexeev, and S. Mardanikorani, "Wireless communication over an LED channel," *IEEE Commun. Mag.*, vol. 58, no. 12, pp. 77–82, Jan. 2021.
[13] S. Mardanikorani, X. Deng, J.-P. M. Linnartz, and A. Khalid, "Compensating dynamic nonlinearities in LED photon emission to enhance optical wireless communication," *IEEE Trans. Veh. Technol.*, vol. 70, no. 2, pp. 1317–1331, Feb. 2021.
[14] J. Linnartz *et al.*, "ELIoT: New features in LiFi for next-generation IoT," in *Proc. Joint Eur. Conf. Netw. Commun. 6G Summit*, 2021, pp. 148–153.
[15] T. E. B. Cunha, J.-P. M. G. Linnartz, and X. Deng, "Achievable rate of LED-based distributed MIMO OWC systems under a per-LED power constraint," in *Proc. 17th Int. Symp. Wireless Commun. Syst.*, 2021, pp. 1–6.
[16] S. M. Kouhini *et al.*, "Distributed MIMO experiment using LiFi over plastic optical fiber," in *Proc. IEEE Globecom Workshops*, 2020, pp. 1–6.
[17] J. Lee, *Discrete Multitone Modulation for Short-Range Optical Communications*. Eindhoven, The Netherlands: Technische Universiteit Eindhoven, 2009.
[18] S. Mardanikorani, X. Deng, and J.-P. M. Linnartz, "Efficiency of power loading strategies for visible light communication," in *Proc. IEEE Globecom Workshops*, 2018, pp. 1–6.
[19] S. Mardanikorani, X. Deng, and J.-P. M. G. Linnartz, "Sub-carrier loading strategies for DCO-OFDM LED communication," *IEEE Trans. Commun.*, vol. 68, no. 2, pp. 1101–1117, Feb. 2020.
[20] S. Mardanikorani and J.-P. M. Linnartz, "Capacity of the first-order low-pass channel with power constraint," in *Proc. Symp. Inf. Theory Signal Process. Benelux*, 2018, pp. 149–153.
[21] J. Lian and M. Brandt-Pearce, "Multiuser MIMO indoor visible light communication system using spatial multiplexing," *J. Lightw. Technol.*, vol. 35, no. 23, pp. 5024–5033, Dec. 2017.
[22] R. Mesleh, H. Elgala, and H. Haas, "Optical spatial modulation," *IEEE/OSA J. Opt. Commun. Netw.*, vol. 3, no. 3, pp. 234–244, 2011.
[23] C. Chen *et al.*, "User-centric MIMO techniques for indoor visible light communication systems," *IEEE Syst. J.*, vol. 14, no. 3, pp. 3202–3213, Sep. 2020.
[24] R. Y. Mesleh, H. Haas, S. Sinanovic, C. W. Ahn, and S. Yun, "Spatial modulation," *IEEE Trans. Veh. Technol.*, vol. 57, no. 4, pp. 2228–2241, Jul. 2008.
[25] J. Lian, Y. Gao, P. Wu, G. Zhu, and Y. Wang, "Indoor MIMO VLC systems using optical orthogonal frequency division multiple access," *Opt. Commun.*, vol. 485, 2021, Art. no. 126728.
[26] X. Deng, S. Mardanikorani, G. Zhou, and J. M. G. Linnartz, "DC-bias for optical OFDM in visible light communications," *IEEE Access*, vol. 7, pp. 98 319–98 330, 2019.
[27] B. Cardiff, M. F. Flanagan, F. Smyth, L. P. Barry, and A. D. Fagan, "On bit and power loading for OFDM over SI-POF," *J. Lightw. Technol.*, vol. 29, no. 10, pp. 1547–1554, May 2011.
[28] J. G. Proakis and M. Salehi, *Digital Communications: Multichannel and Multicarrier Systems*. New York, NY, USA: McGraw-Hill, 2008.
[29] P. M. Butala, H. Elgala, and T. D. Little, "SVD-VLC: A novel capacity maximizing VLC MIMO system architecture under illumination constraints," in *Proc. IEEE Globecom Workshops*, 2013, pp. 1087–1092.
[30] J. R. Hampton, *Introduction to MIMO Communications: Applications of the MIMO Capacity Formula*. Cambridge, U.K.: Cambridge Univ. Press, 2014.
[31] U. F. Siddiqi, O. Narmanlioglu, M. Uysal, and S. M. Sait, "Joint bit and power loading for adaptive MIMO OFDM VLC systems," *Trans. Emerg. Telecommun. Technol.*, vol. 31, no. 7, 2020, Art. no. e3850.
[32] W. X. Fan *et al.*, "Achievable rate of MIMO-OFDM VLC over low-pass channels," in *Proc. IEEE 16th Conf. Ind. Electron. Appl.*, 2021, pp. 1340–1345.
[33] P. Almers, F. Tufvesson, O. Edfors, and A. F. Molisch, "Measured capacity gain using water filling in frequency selective MIMO channels," in *Proc. 13th IEEE Int. Symp. Pers. Indoor Mobile Radio Commun.*, 2002, pp. 1347–1351.
[34] O. Narmanlioglu and M. Uysal, "Limited feedback channel estimation for multi-user massive MIMO visible light communications," in *Proc. IEEE Int. Conf. Commun.*, 2020, pp. 1–7.
[35] J. M. Kahn and J. R. Barry, "Wireless infrared communications," *Proc. IEEE*, vol. 85, no. 2, pp. 265–298, Feb. 1997.
[36] A. Nuwanpriya, S.-W. Ho, and C. S. Chen, "Indoor MIMO visible light communications: Novel angle diversity receivers for mobile users," *IEEE J. Sel. Areas Commun.*, vol. 33, no. 9, pp. 1780–1792, Sep. 2015.
[37] Y. Wang and N. Chi, "Demonstration of high-speed $2\times$ 2 non-imaging MIMO nyquist single carrier visible light communication with frequency domain equalization," *J. Lightw. Technol.*, vol. 32, no. 11, pp. 2087–2093, Jun. 2014.
[38] J.-P. M. G. Linnartz and X. Deng, "Progressing insights in signal processing for optical wireless communications," in *Proc. Symp. Inf. Theory Signal Process.*, 2021, pp. 66–73.
[39] A. Lapidoth, S. M. Moser, and M. Wigger, "On the capacity of free-space optical intensity channels," *IEEE Trans. Inf. Theory*, vol. 55, no. 10, pp. 4449–4461, Oct. 2009.
[40] S. Mardanikorani, X. Deng, and J.-P. M. Linnartz, "Optimization and comparison of M-PAM and optical OFDM modulation for optical wireless communication," *IEEE Open J. Commun. Soc.*, vol. 1, no. 1, pp. 1721–1737, Oct. 2020.
[41] ITU-T Rec. G.9991, "G.VLC: Draft new recommendation ITU-T G.9991," 2014. [Online]. Available: https://www.itu.int/md/T17-SG15-181008-TD-PLEN-0291

Xiong Deng (Member, IEEE) received the M.Eng. degree in communication and information engineering from the University of Electronic Science and Technology of China, Chengdu, China, in 2013, and the Ph.D. degree in optical wireless communications from the Eindhoven University of Technology, Eindhoven, The Netherlands, in 2018. In 2013, he was a Researcher with the Terahertz Science and Technology Research Center, China Academy of Engineering Physics, Mianyang, China, where he was involved in the integrated terahertz communication and imaging system. He was a Guest Researcher with Signify (Philips Lighting) Research, where he was involved in light fidelity. He is currently an Associate Professor with Southwest Jiaotong University, Chengdu, China, and a PostDoc Researcher with the Eindhoven University of Technology. His research interests include the system modeling, digital signal processing, and circuits for intelligent lighting, millimeter wave, microwave photonics, and optical wireless communications.

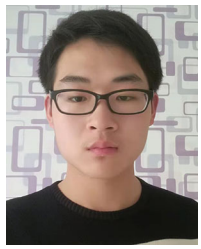

Wenxiang Fan received the B.Eng. degree in electronic information science and technology from the Hunan University of Science and Technology, Xiangtan, China, in 2019. He is currently working toward the M.Eng. degree in optical engineering, with the Institute of Electronic Paper Displays, South China Academy of Advanced Optoelectronics, South China Normal University, Guangzhou, China. He is currently a Visiting Student with the Center for Information Photonics and Communications, Southwest Jiaotong University, Chengdu, China. His research interests include the system modeling, digital signal processing and optical wireless communications.

Authorized licensed use limited to: CHONGQING UNIVERSITY. Downloaded on July 16,2022 at 07:24:30 UTC from IEEE Xplore. Restrictions apply.

Thiago E. Bitencourt Cunha (Member, IEEE) received the B.Sc. degree in telecommunications engineering from Fluminense Federal University, Niterói, Brazil, in 2017 and the M.Sc. degree in electrical engineering from the Pontifical Catholic University of Rio de Janeiro (PUC-Rio), Rio de Janeiro, Brazil, in 2019. He is currently working toward the Ph.D. degree in electrical engineering with the Signal Processing Systems Group, Eindhoven University of Technology (TU/e), Eindhoven, The Netherlands. His research interests include the application of information theory, system modeling, digital signal processing, Internet of Things (IoT), circuits for intelligent lighting and optical wireless communications.

Shuai Ma (Member, IEEE) received the B.S. and Ph.D. degrees in communication and information systems from Xidian University, Xian, China, in 2009 and 2016, respectively. From 2014 to 2015, he was a Visiting Scholar with the Department of Electrical and Com- puter Engineering, Texas A&M University, College Station, TX, USA. he is currently an Associate Professor with the School of Information and Control Engineering, China University of Mining and Technology, Xuzhou, China. His research interests include visible light communication, wireless communications, and network information theory.

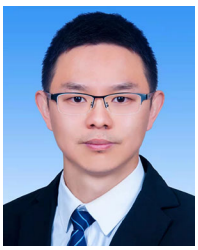

Chen chen (Member, IEEE) received the B.S. and M.Eng. degrees from the University of Electronic Science and Technology of China, Chengdu, China, in 2010 and 2013, respectively, and the Ph.D. degree from Nanyang Technological University, Singapore, in 2017. He was a Postdoctoral Researcher with the School of Electrical and Electronic Engineering, Nanyang Technological University, from 2017 to 2019. He is currently a Tenure-Track Assistant Professor with the School of Microelectronics and Communication Engineering, Chongqing University, Chongqing, China. His research interests include optical wireless communication, optical access networks, Internet of Things, and machine learning.

Yixian Dong received the B.S. and M.Eng. degrees from the University of Electronic Science and Technology of China, Chengdu, China, in 2012 and 2015, respectively, and the Ph.D. degree from Bangor University, Wales, U.K., in 2019. She is currently an Assistant Professor with the Center for Information Photonics & Communications (CIPC), Southwest Jiaotong University, Chengdu, China. Her research interests include short-reach/long-haul optical communications, DSP in optical communications, and convergence of wireless and optical networks.

Xihua Zou (Senior Member, IEEE) is currently a Full Professor and the Deputy Dean with the Center for Information Photonics and Communications, Southwest Jiaotong University, Chengdu, China. He was a Humboldt Research Fellow with the Institute of Optoelectronics, University of Duisburg-Essen, Germany. He was also a Visiting Researcher and a joint training Ph.D. Student with the Microwave Photonics Research Laboratory, University of Ottawa, ON, Canada, and a Visiting Scholar with the Ultrafast Optical Processing Research Group, INRS-EMT, Canada. He has authored or coauthored more than 80 academic papers in high-impact refereed journals, and over ten granted Chinese patents. His research interests include microwave photonics, microwave/millimeter-wave over fiber communication for 5G/B5G, integrated photonics. Dr. Zou was the recipient of the Alexander von Humboldt Research Fellowship, Excellent Young Scholar of NSFC, National Outstanding Expert in Science & Technology of China, the Nomination Award for the National Excellent Doctoral Dissertation of China. He was also the recipient of the OSA 2018 Outstanding Reviewer. He is currently the Associate Editor of the IEEE JOURNAL OF QUANTUM ELECTRONICS, and ISC (International Steering Committee) Member of the IEEE Topical Meeting on Microwave Photonics (MWP). He was the Guest Editor for a Special Issue on Microwave Photonics in IEEE/OSA JOURNAL OF LIGHTWAVE TECHNOLOGY, and the leading Guest Editor for a Special Section on Microwave Photonics in SPIE Optical Engineering.

Lianshan Yan (Senior Member, IEEE) received the B.E. degree from Zhejiang University, Hangzhou, China, and the Ph.D. degree from the University of Southern California (USC), Los Angeles, CA, USA. He is currently the Dean of the School of Information Science & Technology (SIST) and the Director of Center for Information Photonics & Communications (CIPC), Southwest Jiaotong University, Chengdu, China. Prof. Yan is the author and co-author of more than 500 papers, including more than ten invited journal papers and more than fifty invited talks. He also authored three books and two book chapters. He holds 13 issued U.S. patents and more than seventy Chinese patents. Prof. Yan is a Fellow of Optica (formerly OSA). He is the co-Editor-in-Chief of Light: Advanced Manufacturing (2020). He was the recipient of the IEEE Photonics Society Distinguished Lecturer Award (2011–2013) and IEEE LEOS Graduate Fellowship (2002). He was the Co-Chair or TPC Member of more than 50 international conferences. He is also the winner of the National Science Fund for Distinguished Young Scholars of China, Chair Professor of Cheung Kong Scholars Program. He was the Chair of Optical Fiber Technology Technical Group of Optical Society of America (OSA, 2015–2018) and an Associate Editor of IEEE PHOTONICS JOURNAL (2009–2015).

Jean-Paul M. G. Linnartz (Fellow, IEEE) received the M.Sc. degree (*cum laude*) from the Eindhoven University of Technology (TU/e), Eindhoven, The Netherlands, in 1986, and the Ph.D. degree (*cum laude*) from the Delft University of Technology (TU Delft), The Netherlands, in 1991. He was a Senior Director with the Philips Research, Eindhoven, where he headed Security, Connectivity, and IC Design Research Groups. He initiated research on Coded Light, to allow the embedding of identifiers in light sources, which is currently being used in many office and retail facilities. He is currently a part-time Professor with the TU/e, addressing intelligent lighting systems and optical wireless communication, and a Research Fellow with Signify (Philips Lighting) Research. His inventions led to more than 75 granted patent families and have been a basis for three ventures. His papers have been cited more than 12 000 times and his H-index is 53 (GS). From 1992 to 1995, he was an Assistant Professor with the University of California, Berkeley, Berkeley, CA, USA. In 1994, he was an Associate Professor with TU Delft. From 1988 to 1991, he was an Assistant Professor with the TU Delft. He is a Fellow of the IEEE for his leadership in Security with Noisy Data.

Authorized licensed use limited to: CHONGQING UNIVERSITY. Downloaded on July 16,2022 at 07:24:30 UTC from IEEE Xplore. Restrictions apply.